JGR Planets

RESEARCH ARTICLE

10.1029/2018JE005895

**Key Points:**

- The topside ionosphere of Mars is characterized by a common ion density scale height of 100 km on the dayside and 190 km on the nightside
- Strong bulk ion outflow is present on Mars, being supersonic at sufficiently high altitudes and driven by the ambient magnetic pressure
- The ambient magnetic field has an obvious impact on the ion distribution, with distinct patterns on the dayside and the nightside of Mars

**Correspondence to:**
J. Cui,
cuijun7@mail.sysu.edu.cn

**Citation:**
Wu, X.-S., Cui, J., Xu, S. S., Lillis, R. J., Yelle, R. V., Edberg, N. J. T., et al. (2019). The morphology of the topside Martian ionosphere: Implications on bulk ion flow. *Journal of Geophysical Research: Planets*, *124*, 734–751. https://doi.org/10.1029/2018JE005895

Received 3 DEC 2018
Accepted 25 JAN 2019
Accepted article online 13 FEB 2019
Published online 11 MAR 2019



# The Morphology of the Topside Martian Ionosphere: Implications on Bulk Ion Flow

**X.-S. Wu[1,2], J. Cui[1,2,3], S. S. Xu[4], R. J. Lillis[4], R. V. Yelle[5], N. J. T. Edberg[6], E. Vigren[6], Z.-J. Rong[7], K. Fan[7], J.-P. Guo[3], Y.-T. Cao[1], F.-Y. Jiang[1,5], Y. Wei[7], and D. L. Mitchell[4]**

[1]CAS Key Laboratory of Lunar and Deep Space Exploration, Chinese Academy of Sciences, Beijing, China, [2]CAS Center for Excellence in Comparative Planetology, Chinese Academy of Sciences, Hefei, China, [3]School of Atmospheric Sciences, Sun Yat-sen University, Zhuhai, China, [4]Space Sciences Laboratory, University of California, Berkeley, CA, USA, [5]Lunar and Planetary Laboratory, University of Arizona, Tucson, AZ, USA, [6]Swedish Institute of Space Physics, Uppsala, Sweden, [7]Institute of Geology and Geophysics, Chinese Academy of Sciences, Beijing, China

**Abstract** Prior to the Mars Atmosphere and Volatile Evolution mission, the only information on the composition of the Martian ionosphere came from the Viking Retarding Potential Analyzer data, revealing the presence of substantial ion outflow on the dayside of Mars. Extensive measurements made by the Mars Atmosphere and Volatile Evolution Neutral Gas and Ion Mass Spectrometer allow us to examine the morphology of the Martian ionosphere not only in unprecedented detail but also on both the dayside and the nightside of the planet. Above 300 km, various ionospheric species present a roughly constant density scale height around 100 km on the dayside and 180 km on the nightside. An evaluation of the ion force balance, appropriate for regions with near-horizontal magnetic field lines, suggests the presence of supersonic ion outflow predominantly driven by the ambient magnetic pressure, with characteristic dayside and nightside flow velocities of 4 and 20 km/s, respectively, both referred to an altitude of 500 km. The corresponding total ion outflow rates are estimated to be $5 \times 10^{25}$ $s^{-1}$ on the dayside and $1 \times 10^{25}$ $s^{-1}$ on the nightside. The data also indicate a prominent variation with magnetic field orientation in that the ion distribution over regions with near-vertical field lines tends to be more extended on the dayside but more concentrated on the nightside, as compared to regions with near-horizontal field lines. These observations should have important implications on the pattern of ion dynamics in the vicinity of Mars.

**Plain Language Summary** Prior to the Mars Atmosphere and Volatile Evolution mission, the only information on the composition of the Martian ionosphere came from the Viking Retarding Potential Analyzer data acquired on the dayside of Mars. Recently, extensive measurements made by the Mars Atmosphere and Volatile Evolution Neutral Gas and Ion Mass Spectrometer allow us to examine the Martian ionosphere not only in unprecedented detail but also on both the dayside and the nightside of the planet. By analyzing these data, we find that on each side, many of the detected ion species share a common density structure at altitudes above 300 km. Meanwhile, such a structure is clearly influenced by the ambient magnetic fields, which are well known to be inhomogeneous on Mars and cluster over the Southern Hemisphere. Near strong magnetic fields, the Martian ionosphere tends to be more extended on the dayside but more concentrated on the nightside. These findings reveal the presence of supersonic ion outflow on Mars. Such an ion outflow makes a significant contribution to plasma escape, which influences the long-term evolution of the planet.

## 1. Introduction

On the dayside, the Martian ionosphere contains a well-defined primary layer and a low-altitude secondary layer which are mainly produced by solar Extreme Ultraviolet (EUV)/X-ray ionization along with impact ionization by photoelectrons and their secondaries (e.g., Fox & Weber, 2012; Fox & Yeager, 2006, 2009; Martinis et al., 2003; Xu et al., 2018). Near the primary peak, the Martian ionosphere is reasonably described by the idealistic Chapman theory under photochemical equilibrium (e.g., Mendillo et al., 2013, 2015, 2017). Well above this peak, where the effect of ionospheric chemistry is supressed and transport becomes the dominant controlling process (e.g., Němec et al., 2011), existing studies suggest that the ideal diffusive equilibrium condition fails to adequately explain the available measurements of the dayside ionospheric plasma (e.g., Chen et al., 1978; Ergun et al., 2016; Fox, 1997, 2009; Kar et al., 1996).

Comparisons of model ion density profiles with the Viking 1 Retarding Potential Analyzer (RPA) measurements implied a dayside upward flux of $5 \times 10^7$ cm$^{-2}$ s$^{-1}$ for $O_2^+$ and $4 \times 10^6$ cm$^{-2}$ s$^{-1}$ for $O^+$ under solar minimum conditions (Fox, 2009). Early measurements of the $O_2^+$ and $O^+$ distributions in the Martian ionosphere were not available under solar maximum conditions, but radio occultation (RO) measurements made onboard Mariners 6 and 7 were used to constrain the dayside upward flux to be (1.2–1.6) $\times 10^8$ cm$^{-2}$ s$^{-1}$ for $O_2^+$ and (1.5–2) $\times 10^7$ cm$^{-2}$ s$^{-1}$ for $O^+$ (Fox, 2009), respectively. In another study, Shinagawa and Cravens (1989) interpreted the Viking RPA data by incorporating horizontal rather than vertical plasma outflow, analogous to the situation occurring on Venus under high solar wind (SW) dynamical pressures (e.g., Cravens et al., 1984; Luhmann et al., 1984; Phillips et al., 1984; Shinagawa & Cravens, 1988; Shinagawa et al., 1987). The solar cycle variation in ion outflow was also obtained by Cravens et al. (2017) using a semiempirical approach and predicted to scale with the square root of the solar ionizing flux. The inferred dayside plasma outflow either helps to maintain a substantial nightside ionosphere on Mars (e.g., Brain et al., 2015; Cui et al., 2015; Girazian, Mahaffy, Lillis, Benna, Elrod, Jakosky, 2017; Němec et al., 2010; Withers et al., 2012) or leads to considerable plasma escape down the tail (e.g., Barabash et al., 2007; Dubinin, Fraenz, Pätzold, McFadden, et al., 2017; Dubinin, Fraenz, Pätzold, Andrews, et al., 2017; Edberg et al., 2010; Lundin et al., 2013; Ramstad et al., 2015). The relative contributions of these two channels are comparable based on existing magnetohydrodynamic calculations (e.g., Ma et al., 2004).

A further complication lies in the modulation of the topside Martian ionosphere by strong crustal magnetic anomalies known to cluster over the southern hemisphere of the planet (e.g., Acuna et al., 1998, 1999; Connerney et al., 1999). According to the extensive measurements made with the Mars Advanced Radar for Subsurface and Ionospheric Sounding (MARSIS) onboard the Mars Express (MEx) spacecraft, the magnetically controlled regions of the dayside Martian ionosphere are typically manifest as hyperbola-shaped traces in the echogram and dual traces in the ionogram (e.g., Diéval et al., 2018; Duru et al., 2006; Gurnett et al., 2005; Nielsen et al., 2007). These radar signatures were found to be extremely stable and preferentially occur over regions with near-vertical field lines (e.g., Andrews et al., 2014). Such an observation, indicative of upwelling of the ambient ionospheric plasma, was first suggested to be driven by SW electron precipitation (Gurnett et al., 2005), but this scenario was later disputed because simultaneous measurements revealed no signature of shocked SW plasma for a significant portion of the upwelling events (Diéval et al., 2015). Instead, the ionospheric upwelling was argued to be a natural outcome of field-aligned plasma diffusion without the need to invoke external SW electron precipitation (Matta et al., 2015). The above scenario is consistent with the early RO measurements made by Mars Global Surveyor (MGS), revealing a reduced electron density scale height well above the main peak of the dayside Martian ionosphere over regions with preferentially horizontal magnetic field lines (e.g., Ness et al., 2000). Such a feature was also demonstrated by the more recent MEx MARSIS radar data (Ramírez-Nicolás et al., 2016).

On the nightside, the magnetic control of the Martian ionosphere is manifest as reduced electron impact ionization rates near strong crustal anomalies (e.g., Lillis et al., 2009, 2011, 2018), where existing observations indicate reduced energetic electron fluxes over a range of electron energy and under a range of SW conditions (e.g., Lillis & Brain, 2013). Energetic electron depletion is frequently seen on the nightside of Mars indicative of closed field lines effectively shielding the precipitation of SW electrons (e.g., Steckiewicz et al., 2015, 2017), and such regions are preferentially located near strong crustal anomalies (Xu, Mitchell, Liemohn, et al., 2017). The incident electron flux also increases as the field lines are more vertical (Lillis & Brain, 2013; Lillis et al., 2018), which is responsible for the apparent correlation between magnetic orientation and ionospheric electron content as revealed by the MEx MARSIS data (Safaeinili et al., 2007).

Previous studies of the topside Martian ionosphere largely relied on electron density profiles extracted from either the MARSIS measurements made by MEx (Gurnett et al., 2008) or the RO measurements made by both MGS (Tyler et al., 2001) and MEx (Pätzold et al., 2016). Knowledge of the ion composition and distribution was generally not available except for two individual ion density profiles measured by the Viking RPA on the dayside of Mars (Hanson et al., 1977). This situation has been significantly improved by the Mars Atmosphere and Volatile Evolution (MAVEN) mission (Jakosky et al., 2015) with its Neutral Gas and Ion Mass Spectrometer (NGIMS) providing, in the open source ion (OSI) mode, a wealth of information on the densities of many important species of the Martian ionosphere covering a broad mass range of 2–150 Da (Mahaffy, Benna, King, et al., 2015). Meanwhile, the available NGIMS measurements extend well beyond the terminator (e.g., Girazian, Mahaffy, Lillis, Benna, Elrod, Jakosky, et al., 2017; Girazian, Mahaffy, Lillis,

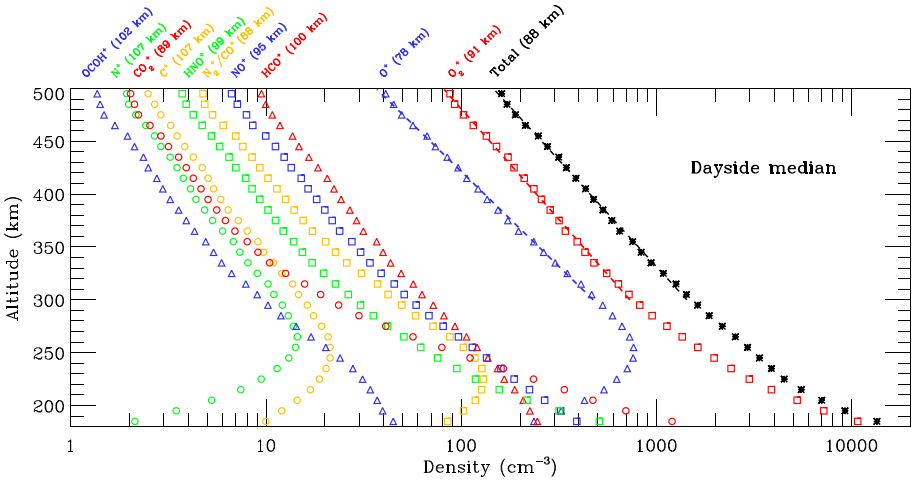


**Figure 1.** The median altitude profiles of 10 important ion species in the dayside Martian ionosphere at 180–500 km, obtained with 3.5 years of MAVEN NGIMS observations. The median total ion density profile is displayed by the asterisks. The identification of the ion species is adapted from Benna, Mahaffy, Grebowsky, Fox, et al. (2015) and indicated at the top of the figure. The numbers in the parentheses refer to the topside ion density scale heights in kilometers obtained by exponential fittings to the NGIMS ion density data above 300 km. Example fits to the $O_2^+$, $O^+$, and total ion density profiles at 300–500 km are shown with the dashed lines.

Benna, Elrod, Fowler, et al., 2017), allowing a thorough investigation of the topside Martian ionosphere on the nightside.

The data acquired by the NGIMS were used to explore the characteristics of the Martian ionosphere under a range of external conditions (e.g., Benna, Mahaffy, Grebowsky, Fox, et al., 2015; Benna, Mahaffy, Grebowsky, Plane, et al., 2015; Girazian, Mahaffy, Lillis, Benna, Elrod, Jakosky, et al., 2017; Girazian, Mahaffy, Lillis, Benna, Elrod, Fowler, et al., 2017; Vogt et al., 2015; Withers, Vogt, Mahaffy, et al., 2015; Withers, Vogt, Mayyasi, et al., 2015). In the present study, the NGIMS OSI level 2 data from the arrival of MAVEN at Mars on 21 September 2014 to 14 February 2018 are used. The available NGIMS ion density data cover the altitude range from the nominal periapsis at 140–180 up to 500 km for the majority of MAVEN orbits during the nominal mission (Jakosky et al., 2015), to be distinguished from the coverage of the Viking RPA ion density data that does not extend above 300 km (Hanson et al., 1977).

The layout of the paper is as follows. We present in section 2 the dayside and the nightside median profiles of a sequence of important species of the Martian ionosphere, with an emphasis placed on the observed topside ion density scale heights. We then examine in section 3 the impact of the magnetic field configuration, distinguishing between two cases with near-horizontal and near-vertical field lines. This is followed by section 4 where we evaluate the force balance of various species in the Martian ionosphere, which allows the characteristics of the bulk ion flow to be inferred and the flow velocities to be estimated. Finally, we discuss our results in section 5 and provide concluding remarks in section 6.

## 2. The Median Morphology of the Martian Ionosphere

We show in Figure 1 the dayside median morphology of the Martian ionosphere, defined as SZA < 90°, over the altitude range from 180 to 500 km in terms of the number density profiles of 10 important ion species following the identification scheme of Benna, Mahaffy, Grebowsky, Fox, et al. (2015). These species are $O_2^+$, $O^+$, $HCO^+$, $NO^+$, $N_2^+/CO^+$, $HNO^+$, $C^+$, $CO_2^+$, $N^+$, and $OCOH^+$, respectively, in decreasing order of dayside median density at 500 km. We caution that the NGIMS is incapable of distinguishing between $N_2^+$ and $CO^+$ in the OSI mode due to their equality in mass. The median vertical profile of the electron number density, assumed to be identical to the total ion number density, is displayed by the asterisks in the same figure. Distinctive layer structures are manifest in a portion of ion species including $O^+$, $CO^+/N_2^+$, $C^+$, and $N^+$, whereas for the remaining ion species, their respective peak altitudes are located below the vertical extent displayed in the figure (e.g., Chen et al., 1978; Fox, 2003, 2004, 2009; Fox et al., 2015; González-Galindo et al., 2013; Shinagawa & Cravens, 1989; Matta et al., 2013).

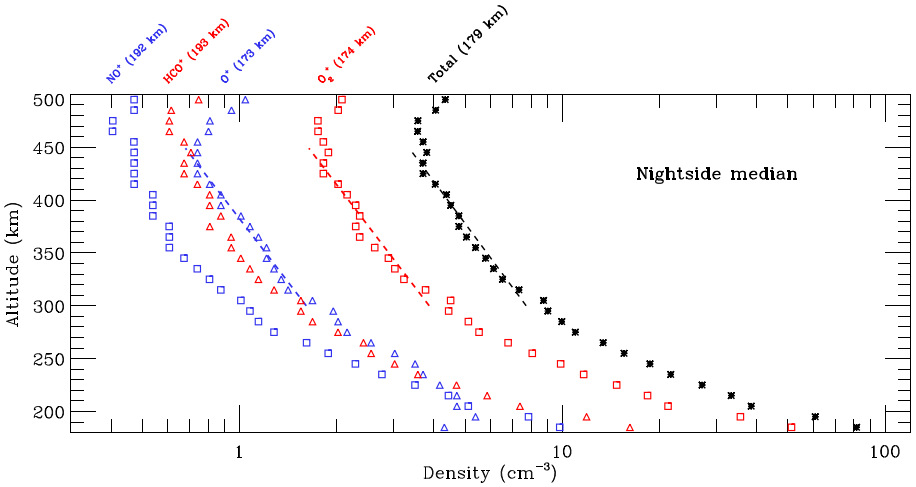


**Figure 2.** Similar to Figure 1 but for the nightside Martian ionosphere.

From Figure 1, all ion species tend to decline exponentially with increasing altitude well above the primary peak, featured by a more or less constant density scale height. As a crude estimate, an exponential fit is performed to the density distribution of each ion species from 300 km to the top boundary, which provides information on the median topside ion density scale height on the dayside of Mars. These scale heights in kilometers are provided at the top of Figure 1 for reference. Interestingly, all ion species demonstrate a quite uniform topside density scale height around 100 km with a scattering of only 10% over a fairly broad mass range of 12–45 Da. The scale height for electron density or total ion density is near 90 km. In Figure 1, we

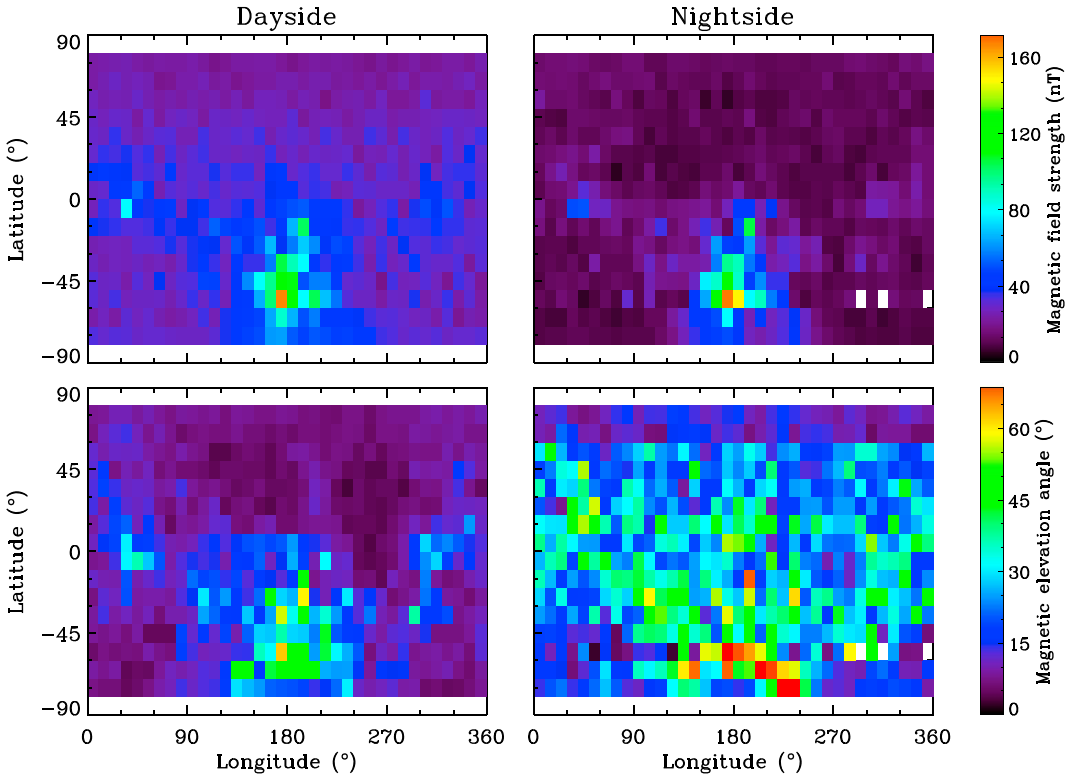


**Figure 3.** The mappings of both the magnetic field strength (top row) and elevation angle (bottom row), based on the Mars Atmosphere and Volatile Evolution Magnetometer level 2 data at 350–450 km, left for the dayside and right for the nightside, respectively.

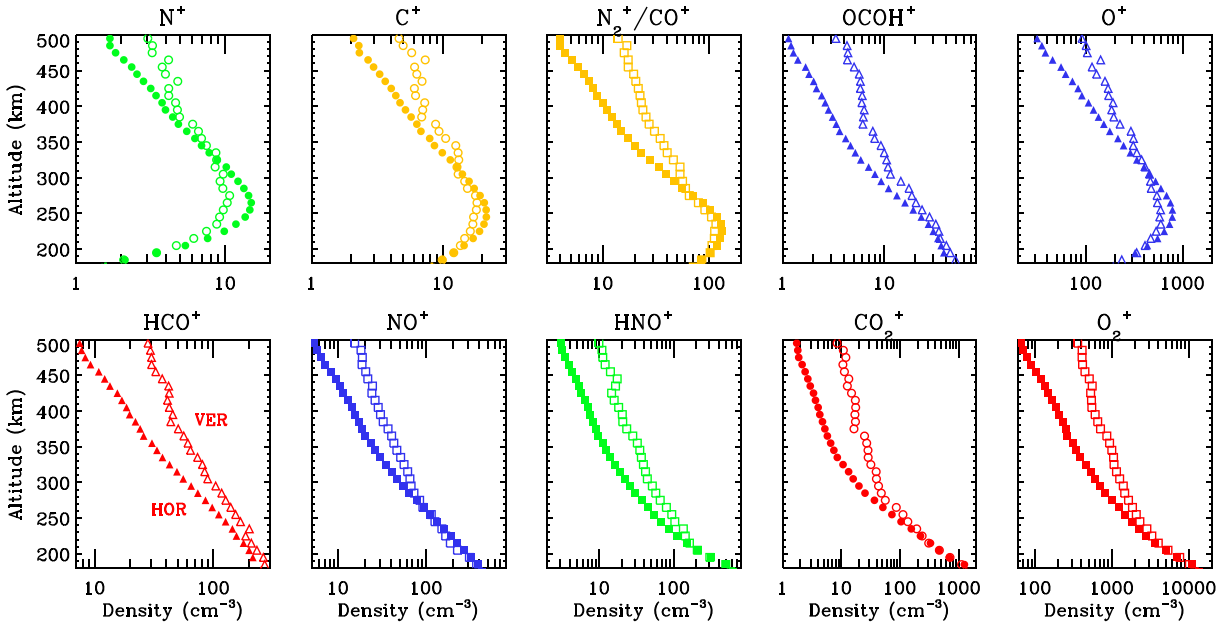


**Figure 4.** The median altitude profiles of 10 important ion species in the dayside Martian ionosphere at 180–500 km, obtained with 3.5 years of Mars Atmosphere and Volatile Evolution Neutral Gas and Ion Mass Spectrometer observations. The identification of the ion species is adapted from Benna, Mahaffy, Grebowsky, Fox, et al. (2015) and indicated at the top of each panel for reference. The open and solid symbols, following the drawing convention of Figure 1, characterize the near-vertical (VER) and near-horizontal (HOR) magnetic field configurations, respectively, defined with the magnetic elevation angle above 60° and below 30°.

display with the dashed lines the exponential fits to the dayside median profiles of the $O_2^+$, $O^+$, and total ion densities at 300–500 km.

We ought to mention that Benna, Mahaffy, Grebowsky, Fox, et al. (2015) reported the detection of substantially more ion species based on the available NGIMS measurements, but many of these species are neglected here because photochemical processes are likely important at altitudes above 300 km, such as $H_2^+$, $H_3^+$, $OH^+$, $H_2O^+$, and $H_3O^+$. This could be viewed from their apparent density peaks typically located at 350–400 km (e.g., Fox et al., 2015; Matta et al., 2013). Other ion species including $He^+$, $CH^+$, $NH^+$, $Ar^+$, and $ArH^+$ are also neglected because their dayside median densities remain below 1 $cm^{-3}$ over a significant portion of the altitude range displayed in Figure 1 (e.g., Benna, Mahaffy, Grebowsky, Fox, et al., 2015), and the accurate determination of their topside density scale heights is thus problematic.

We next explore the median morphology of the Martian ionosphere on the nightside, defined as SZA >120°. This SZA choice ensures that all nightside ion density profiles are completely located within the optical shadow up to the top boundary of 500 km. Here we consider four ion species including $O_2^+$, $O^+$, $HCO^+$, and $NO^+$ in decreasing order of nightside median density at 500 km, with the remaining species displayed in Figure 1 neglected due to their relatively low densities at all altitudes sampled by the NGIMS. The nightside median density profiles for the four species are shown in Figure 2 at 180–500 km, which are generally consistent with the published nightside NGIMS ion density results (e.g., Girazian, Mahaffy, Lillis, Benna, Elrod, Jakosky, et al., 2017; Girazian, Mahaffy, Lillis, Benna, Elrod, Fowler, et al., 2017). Except for regions above 450 km, these species roughly present an exponential decay with increasing altitude, though their density scale heights are not as constant as on the dayside. Exponential fittings are performed to the density profiles in Figure 2 between 300 and 450 km, from which a characteristic topside density scale height could be obtained for each ion species. These scale heights are provided at the top of Figure 2 for reference, revealing a fairly common scale height with a scattering of 6% only. The scale height for the electron density or total ion density is close to 180 km. Similar to Figure 1, we display with the dashed lines the exponential fits to the nightside median profiles of the $O_2^+$, $O^+$, and total ion densities at 300–450 km in Figure 2.

## 3. Impacts of the Magnetic Field Configuration

Mars is unique among terrestrial planets in its possession of multiple magnetic anomalies of small spatial scale in the crust (e.g., Acuna et al., 1998, 1999; Connerney et al., 1999), which leads to a complex pattern

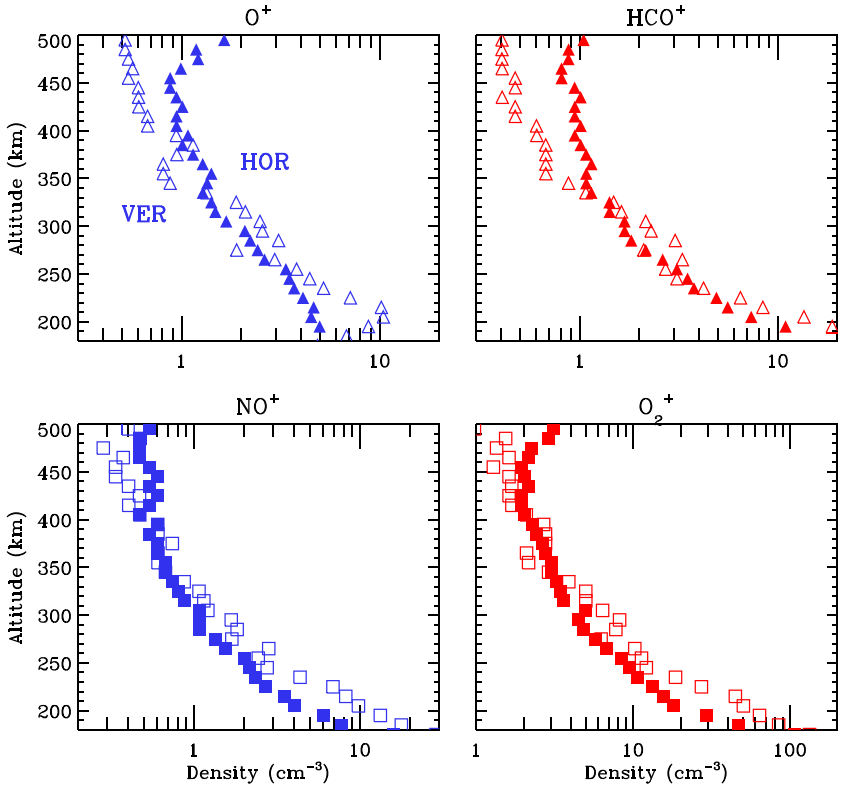


**Figure 5.** Similar to Figure 4 but for the nightside Martian ionosphere.

of ambient magnetic field configuration in the vicinity of the planet (e.g., Harada et al., 2018; Lillis et al., 2004; Mitchell et al., 2001; Weber et al., 2017; Xu, Mitchell, Liemohn, et al., 2017, Xu, Mitchell, Luhmann, et al., 2017). The dayside and nightside mappings of both the magnetic field strength and elevation angle are displayed in Figure 3, extracted from the MAVEN Magnetometer level 2 data at 350–450 km (Connerney et al., 2015). The elevation angle is defined as the angle that the magnetic field line makes with the local horizontal plane. The dayside mapping is to be compared with Figure 12 of Xu, Mitchell, Liemohn, et al. (2017) for a different altitude coverage, revealing a clear correlation between the magnetic field strength and elevation angle in that more vertical field lines tend to cluster around strong magnetic anomalies on Mars, especially near Terra Cimmeria (e.g., Langlais et al., 2004). In contrast, such vertical field lines are observed over a fairly extended region on the nightside. We consider in this study two cases, one with near-vertical magnetic elevation above 60° and the other one with near-horizontal magnetic elevation below 30°.

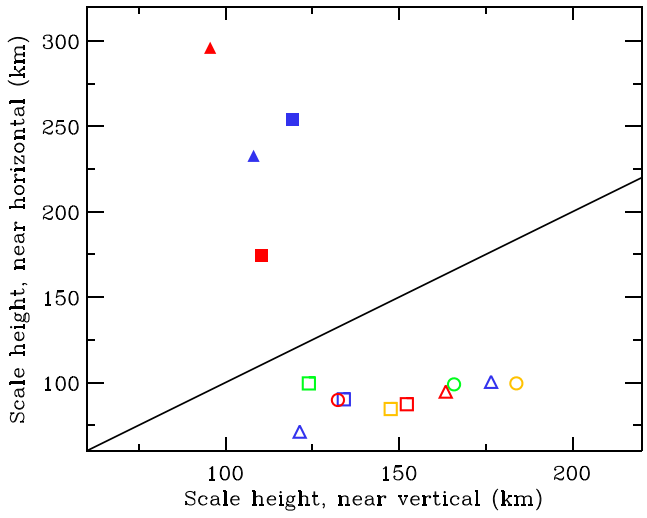


**Figure 6.** A comparison in the observed topside ion density scale height above 300 km in the Martian ionosphere between the near-vertical and near-horizontal magnetic field configurations, defined with the magnetic elevation angle above 60° and below 30°. The drawing convention is the same as in Figures 1 and 3 with the open and filled symbols standing for the dayside and nightside species, respectively.

On the dayside, the median density profiles of various species in the Martian ionosphere for the above two cases are compared in Figure 4, revealing a prominent variation with the magnetic field orientation in that the ion distributions for near-vertical field lines tend to be more extended than those for near-horizontal field lines. On average, the scale heights for the former case are greater than those for the latter case by 70%. The maximum difference is 85% for $C^+$ and the minimum difference is 25% for $HNO^+$, respectively.

Switching to the nightside, the impact of the magnetic field configuration is observed to be remarkably different from the dayside, as revealed by the median ion density profiles shown in Figure 5. For each of the nightside species, the NGIMS ion density scale height for near-vertical field lines

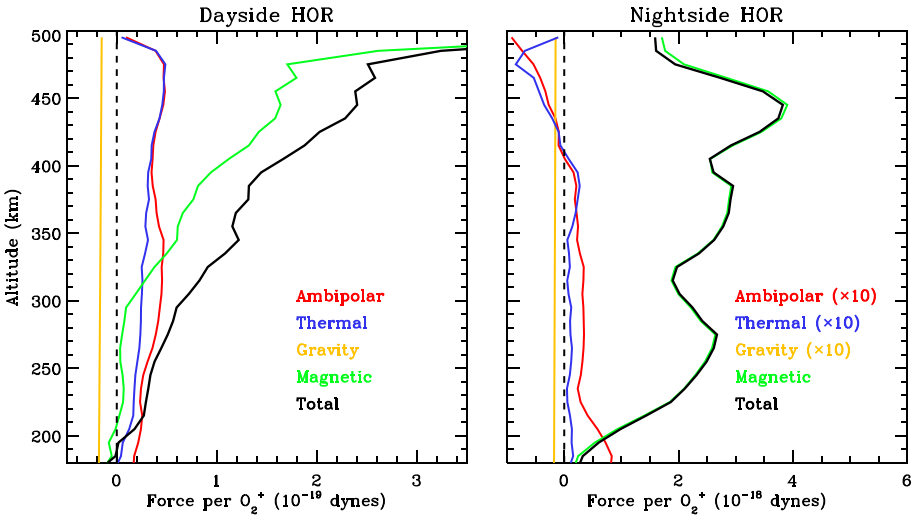


**Figure 7.** The median altitude profiles of vertical force per $O_2^+$ ion in the Martian ionosphere, restricted to regions with near-horizontal (HOR) magnetic field lines, left for the dayside and right for the nightside, respectively. Different colors stand for different force terms in equation (1), blue for the ion thermal pressure, red for the ambipolar electric field, orange for the local gravity, green for the magnetic pressure, and black for the sum of all terms, respectively.

tends to be smaller than the respective scale height for near-horizontal field lines, in direct opposite to the dayside trend. The difference in scale height between the two cases varies from species to species, with a maximum difference of around 70% observed for $HCO^+$ and a minimum difference of around 40% observed for $O_2^+$, respectively.

A direct comparison in the topside ion density scale height between near-horizontal and near-vertical field lines is displayed in Figure 6, with the solid line corresponding to identical scale height between the two cases. The figure demonstrates clearly the opposite impacts of the magnetic field configuration on the median morphology of the topside Martian ionosphere. On the dayside, the available NGIMS observations are generally consistent with the early finding of a smaller dayside electron density scale height over regions with near-horizontal field lines above the primary peak based on the MGS RO measurements (Ness et al., 2000) and imply that the magnetic field orientation crucially controls the distribution of the ambient ionospheric plasma (e.g., Matta et al., 2015). Of more interest is our finding of the opposite trend on the nightside which has not been reported in any previous works. Combining the NGIMS observations on both hemispheres has important implications on the pattern of ion dynamics in the vicinity of Mars.

## 4. Force Balance and Implications on Bulk Ion Flow

Clues to the characteristics of the bulk ion flow can be gained by evaluating the force balance of various species in the topside Martian ionosphere. Assuming diffusive equilibrium in the vertical direction, the total vertical force per ion, $f_i$, for a given species, $i$, could be written as

$$f_i = -\frac{1}{n_i}\frac{d(n_i k T_i)}{dz} - \frac{1}{n_e}\frac{d(n_e k T_e)}{dz} - m_i g - \frac{1}{n_e}\frac{d}{dz}\left(\frac{B_h^2}{8\pi}\right), \quad (1)$$

where $z$ is the altitude, $n_i$ and $n_e$ are the ion and electron number densities, $T_i$ and $T_e$ are the ion and electron temperatures, $m_i$ is the ion mass, $k$ is the Boltzmann constant, $g$ is the local gravity, and $B_h$ is the horizontal magnetic field strength. Various terms on the right-hand side of equation (1) represent the contributions from the ion thermal pressure, the ambipolar electric field, the local gravity, as well as the magnetic pressure, respectively. Equation (1) is analogous to the vertical ion momentum equation used by Fox (2009) with the extra inclusion of the magnetic pressure gradient force, which we show below to be crucial for driving the bulk ion flow. Note that the magnetic mirror force is not included in the ion momentum equation since for isotropic plasma, it is exactly balanced by the part of the pressure force associated with the changing area of the flux tube (Comfort, 1988).

The derivation of equation (1) is provided in Appendix A for completeness. One crucial approximation used in reaching the equation is that the ambient magnetic fields are near horizontal with negligible vertical

components. According to existing observations (e.g., Akalin et al., 2010; Brain et al., 2006; Connerney et al., 2015; Mitchell et al., 2001; Xu, Mitchell, Liemohn, et al., 2017) and model calculations (e.g., Ma et al., 2002, 2004, 2014), such an approximation reasonably describes the magnetic field topology in the vicinity of Mars except for restricted regions near strong crustal magnetic anomalies (see also Figure 3).

The electron and ion temperatures in equation (1) could be determined from measurements of the current voltage characteristics made with the MAVEN Langmuir Probe and Waves (Andersson et al., 2015) and measurements of the thermal $O_2^+$ energy spectra made with the MAVEN Suprathermal and Thermal Ion Composition (McFadden et al., 2015). The complete set of derived ion temperatures is currently not available to us, and accordingly, the ion temperature is parameterized in a crude manner in that it is assumed to be everywhere equal to the electron temperature above 350 km but declines linearly to the neutral temperature at 180 km (e.g., Chen et al., 1978; Choi et al., 1998; Matta et al., 2015; Sakai et al., 2016). Here the neutral temperature is obtained from the isothermal fitting to the respective $CO_2$ densities measured by the NGIMS in the Closed Source Neutral mode (Mahaffy, Benna, Elrod, et al., 2015). Only the inbound NGIMS data are used to avoid possible contamination by wall adsorption and chemistry (Cui et al., 2018). The above parameterization of the ion temperature is likely subject to considerable uncertainties, but these uncertainties should not be important for the purpose of the present study due to the dominance of the magnetic pressure gradient force (see below).

The ion force balance in the dayside Martian ionosphere is displayed in the left panel of Figure 7, taking $O_2^+$ as an example and restricted to regions with near-horizontal field lines. Different colors stand for different force terms, blue for the ion thermal pressure, red for the ambipolar electric field, orange for the local gravity, green for the magnetic pressure, and black for the sum of all terms, respectively. Based on the figure, the dayside $O_2^+$ force balance is dominated by ambipolar electric field below 330 km and by magnetic pressure above. The contributions from local gravity and ion thermal pressure are also important at relatively low altitudes. When switching to the nightside where the ion and electron densities fall by more than an order of magnitude as compared to the dayside, the $O_2^+$ force balance is almost exclusively contributed by magnetic pressure, with the summed contribution from the remaining force terms in equation (1) being on average around 2% only. Such a situation is depicted in the right panel of Figure 7, again appropriate for regions with near-horizontal field lines. Clearly, the net force exerted on $O_2^+$ in the topside Martian ionosphere is always outward, implying bulk $O_2^+$ outflow from both the dayside and the nightside of the planet.

Without showing the details, we mention that the $O_2^+$ force balance in regions with near-horizontal field lines depicted above is quite representative of all species considered here, on both the dayside and the nightside of Mars. This is clearly related to the dominant role of magnetic pressure as revealed in Figure 7. Modest divergence in force per ion is present below 300 km on the dayside, which should be connected to the enhanced importance of species-dependent force terms such as the local gravity and the thermal ion pressure at these altitudes. Such a situation is to be distinguished from that occurring in the ionosphere of Titan, for which the role of magnetic pressure is of minor importance except for nightside regions above 1,500 km (Cui et al., 2010).

It is instructive to estimate the appropriate ion flow velocities of various species of the Martian ionosphere. As an initial attempt, we assume diffusion approximation and estimate the ion flow velocity, hereafter denoted as $W_i$, from $W_i \sim f_i/m_i\nu_{in}$, where $\nu_{in}$ is the total ion-neutral momentum transfer collision frequency calculated from the kinetic theory (Schunk, 1977) using the $CO_2$ and O densities measured by the MAVEN NGIMS. Taking dayside $O_2^+$ as an example and for a reference altitude of 300 km, Figure 7 suggests a total upward force per ion of $\sim 7 \times 10^{-20}$ dynes on the dayside of Mars for regions with near-horizontal field lines. This force predicts an $O_2^+$ outflow velocity of $\sim$ 25 km/s at 300 km, where the appropriate total ion-neutral collision frequency of $\sim 5 \times 10^{-4}$ s$^{-1}$ is used. Such an $O_2^+$ outflow velocity is much greater than the respective ion acoustic velocity of $\sim$ 1 km/s at the same altitude, implying that the $O_2^+$ outflow is highly supersonic and the diffusion approximation fails enormously. Estimates made for the other dayside species as well as on the nightside lead to essentially the same conclusion. The supersonic nature of the ion outflow also ensures that the application of the fluid approximation is reasonably valid even though the high-altitude regions under consideration are above the ion exobase.

The above discussion suggests that the advection term cannot be neglected in the ion momentum equation. Here we estimate the ion flow velocity at a reference altitude of 500 km by column integrating the vertical ion

**Table 1**
*The Ion Outflow Velocities and Fluxes at 500 Km Derived From the Multiinstrument MAVEN Data Set for Various Species in the Martian Ionosphere, Appropriate for Regions With Near-Horizontal Magnetic Field Lines and Distinguishing Between the Dayside and the Nightside*

| | Mass | Dayside | | Nightside | |
|---|---|---|---|---|---|
| Species | Dalton | km/s | $cm^{-2}\ s^{-1}$ | km/s | $cm^{-2}\ s^{-1}$ |
| $O_2^+$ | 32 | 3.8 (3.4) | $2.4 \times 10^7$ | 17 (14) | $5.4 \times 10^6$ |
| $O^+$ | 16 | 5.4 (3.4) | $1.6 \times 10^7$ | 24 (14) | $4.4 \times 10^6$ |
| $HCO^+$ | 29 | 3.9 (3.3) | $2.9 \times 10^6$ | 18 (14) | $2.0 \times 10^6$ |
| $NO^+$ | 30 | 3.9 (3.4) | $2.0 \times 10^6$ | 17 (14) | $9.9 \times 10^5$ |
| $N_2^+/CO^+$ | 28 | 4.0 (3.4) | $1.6 \times 10^6$ | — | |
| $HNO^+$ | 31 | 3.8 (3.4) | $1.2 \times 10^6$ | — | |
| $C^+$ | 12 | 6.0 (3.3) | $1.2 \times 10^6$ | — | |
| $CO_2^+$ | 44 | 3.3 (3.4) | $5.6 \times 10^5$ | — | |
| $N^+$ | 14 | 5.4 (3.2) | $9.1 \times 10^5$ | — | |
| $OCOH^+$ | 45 | 3.0 (3.2) | $3.4 \times 10^5$ | — | |

*Note.* The values in the parentheses indicate the corresponding Mach numbers. MAVEN = Mars Atmosphere and Volatile Evolution.

momentum equation (see equation (A8) in Appendix A) from the lower boundary of 180 km, formulated as

$$\frac{1}{2} m_i W_i(500\ \text{km})^2 = \int_{180\ \text{km}}^{500\ \text{km}} f_i(z) dz, \tag{2}$$

where $f_i$ is calculated with equation (1) and the effect of ion-neutral collisions is implicitly ignored (see also section 5). Such a formulism is analogous to the high-altitude approximation of Cravens et al. (2017).

The ion flow velocities at 500 km, obtained with equation (2), are listed in Table 1, characterizing both the dayside and the nightside of Mars for regions with near-horizontal field lines. The values in the parentheses indicate the corresponding Mach numbers, calculated by dividing the estimated flow velocities by the appropriate ion acoustic velocities. Table 1 reveals a relatively small variability in the ion flow velocity at 500 km of around 25% on the dayside and less than 20% on the nightside, respectively. The bulk ion outflow is supersonic, with a nearly species-independent Mach number of 3.3 on the dayside and as large as 14 on the nightside. The constancy in the Mach number is not surprising since equation (2) predicts that, in view of the dominance of the species-independent magnetic pressure term in equation (1), the ion outflow velocity inversely scales with the square root of the ion mass, that is, $W_i(500\ \text{km}) \propto m_i^{-1/2}$, a scaling relation that also holds for the ion acoustic velocity. For reference, we display in Figure 8 the relation between the ion flow velocity at 500 km and the ion mass, red for the dayside and blue for the nightside, respectively. The solid lines in the figure correspond to the best fit $m_i^{-1/2}$ scaling relations. The dominance of magnetic pressure over thermal pressure implies that the Alfvén velocity is significantly higher than the ion acoustic velocity. For instance, the $O_2^+$ Alfvén velocity can be estimated to increase steadily from ~ 3 km/s at 300 km to ~ 10 km/s at 500 km, over dayside regions with near-horizontal field lines. The outward fluxes for the ion species considered here are also provided in Table 1. In contrast to the ion outflow velocity, the ion outward flux varies substantially among different species, in response to the large variability in ion density.

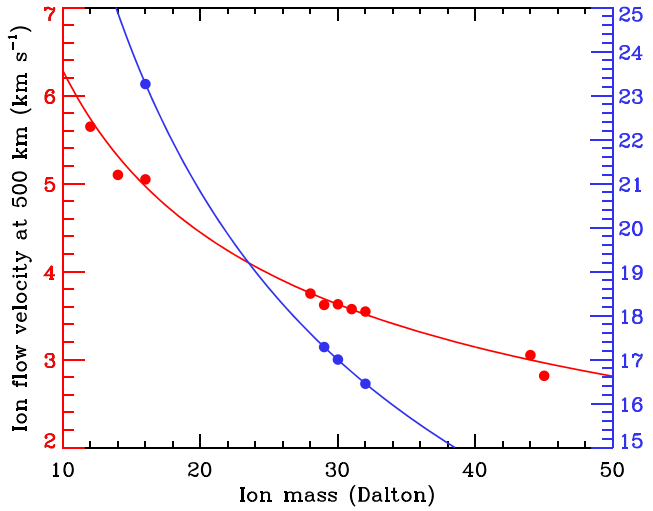


**Figure 8.** The ion flow velocity at 500 km in the topside Martian ionosphere as a function of the ion mass, red for the dayside and blue for the nightside, both appropriate for regions with near-horizontal magnetic field lines. The ion flow velocity is supersonic and scales inversely with the square root of the ion mass.

We caution that equation (2), which involves species-dependent terms such as the local gravity term, the thermal ion pressure term, as well as the advection term, could be used to determine a single flow velocity profile for each ion species, but the equation is obtained by assuming a common

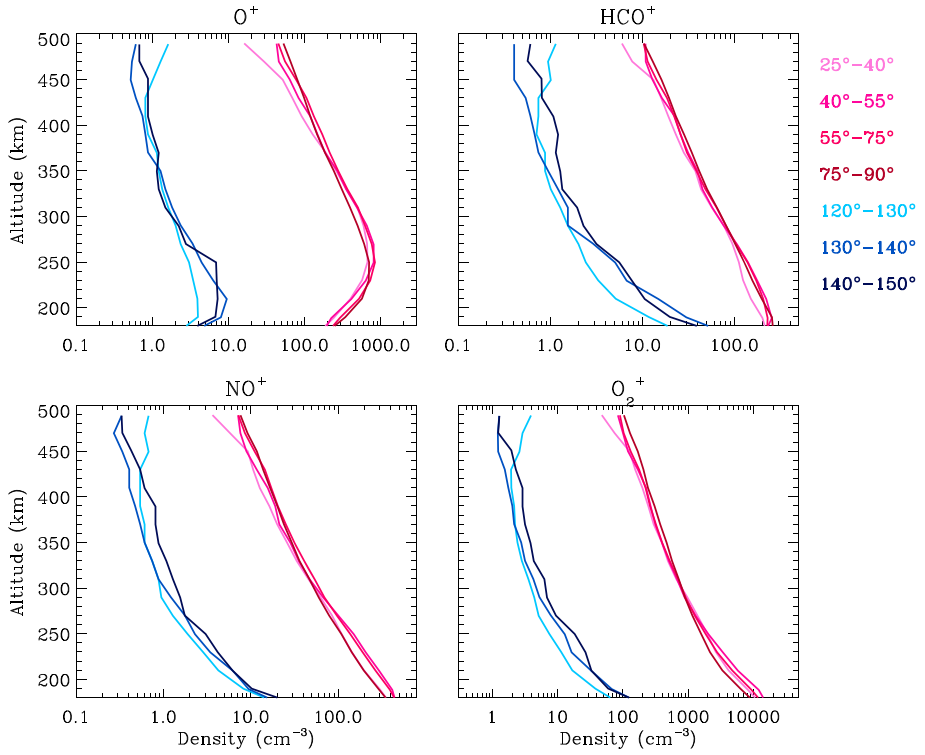


**Figure 9.** The density profiles for four representative ion species, $O^+$, $HCO^+$, $NO^+$, and $O_2^+$, obtained within a sequence of SZA intervals on both the dayside (red) and the nightside (blue) of Mars.

flow velocity profile valid for all species (see Appendix A). Such an assumption is acceptable as the results presented above do indicate that the difference in the predicted ion flow velocities is small.

We emphasize again that the evaluation of the ion force balance presented so far is only appropriate for regions characterized by near-horizontal field lines. With the calculations approximated here, it is difficult to draw firm conclusions on the pattern of ion dynamics in the Martian ionosphere near strong crustal magnetic anomalies, for which equations (1) and (2) are no longer valid due to the presence of substantial vertical field components. A rigorous evaluation of the ion force balance near crustal anomalies requires the inclusion of the magnetic tension force, which further requires the horizontal gradients of the ambient magnetic field components to be calculated. Such a topic is left for follow-up studies.

## 5. Discussions

In this study, a multiinstrument MAVEN data set is used to explore the morphology of the Martian ionosphere over the altitude range of 180–500 km, with an emphasis placed on the topside regions where the effect of chemistry is unimportant and transport becomes the dominant controlling process (e.g., Chen et al., 1978; Fox, 1997, 2009; Matta et al., 2015). On the dayside, a total number of 10 ion species is considered, including $O_2^+$, $O^+$, $HCO^+$, $NO^+$, $N_2^+/CO^+$, $HNO^+$, $C^+$, $CO_2^+$, $N^+$, and $OCOH^+$. Among these species, the first four are also studied on the nightside, defined as SZA above 120°. On both sides, the available NGIMS data reveal that the median densities of all ion species decay exponentially with a more or less constant scale height above 300 km. This density scale height is around 100 km on the dayside with a variability of 10% and around 180 km on the nightside with a variability of only 6%.

It is well known that the morphology of the Martian ionosphere is modulated by the presence of crustal magnetic anomalies clustering over the southern hemisphere of the planet (e.g., Andrews et al., 2014; Diéval et al., 2015, 2018; Duru et al., 2006; Edberg et al., 2008; Gurnett et al., 2005; Nielsen et al., 2007). The impact of the ambient magnetic field configuration is also examined in this study by comparing two categories of topside ionospheric regions, one characterized by near-vertical field lines with magnetic elevation angle above 60° and the other one characterized by near-horizontal field lines with magnetic elevation

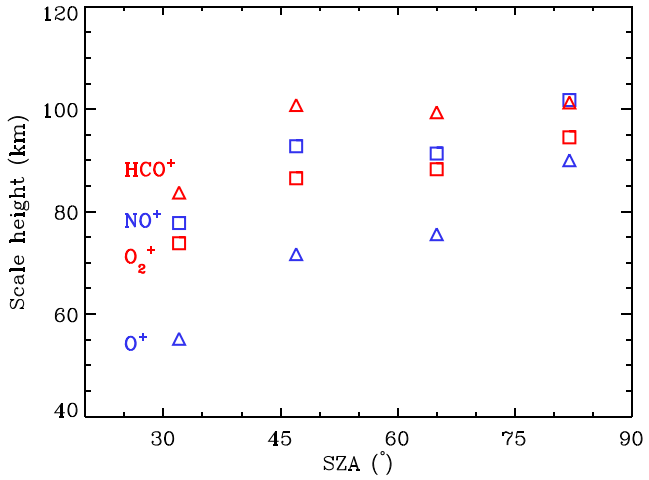


**Figure 10.** The topside ion density scale heights for four representative ion species, $O^+$, $HCO^+$, $NO^+$, and $O_2^+$, all as a function of SZA in the dayside Martian ionosphere. The drawing convention is the same as in Figures 1 and 2.

angle below 30°, respectively. Our analysis reveals a substantially less extended ion distribution on the dayside of Mars over regions with near-horizontal field lines, consistent with the early finding of reduced topside electron density scale height over the same regions (Ness et al., 2000). On the nightside, the impact of the ambient magnetic field configuration is remarkably different in that a less extended ion distribution is observed over regions with near-vertical field lines. The combination of the above observations should have important implications on the pattern of ion dynamics in the vicinity of Mars.

It is necessary to examine how representative the derived ion density scale heights are, in view of the possible variability of the topside Martian ionosphere on both the dayside (Benna, Mahaffy, Grebowsky, Fox, et al., 2015) and the nightside (Girazian, Mahaffy, Lillis, Benna, Elrod, Jakosky, et al., 2017; Girazian, Mahaffy, Lillis, Benna, Elrod, Fowler, et al., 2017). The dayside density profiles for four ion species, $O^+$, $HCO^+$, $NO^+$, and $O_2^+$, are shown in Figure 9, obtained within a sequence of SZA intervals. In response to the relatively small variability in the dayside ion distribution as revealed by the figure, the topside ion density scale heights at 300–500 km also show a small variability, typically at the level of 10% (for $NO^+$) to 20% (for $HCO^+$). We show in Figure 10 the topside ion density scale heights as a function of SZA for the four species displayed in Figure 9, revealing a clear trend of increasing scale height as approaching the terminator. This is consistent with the previous finding of a similar SZA variation in topside electron density scale height, as reported by Andrews et al. (2015). The range of total ion density scale height inferred from Figure 10 is below the range of 80–145 km reported by Duru et al. (2008) based on the MEx MARSIS measurements of the excitation of local electron plasma oscillations, but we should be cautious that the Duru et al. (2008) values were derived for a much higher altitude range of 275–1300 km. The above discussion indicates that the ion density scale heights derived in section 2 are quite representative of the dayside situation. The scale heights quoted in Figure 1 appear to more closely characterize the SZA range of 60–70°, which is not surprising since the dayside NGIMS measurements preferentially sample large SZA regions. We also compare the topside ion density scale heights between regions with near-vertical and near-horizontal field lines, for each of the SZA interval shown in Figure 9. This is demonstrated in Figure 11 taking $O^+$ as an example, from which we conclude that the impact of the ambient magnetic field configuration on the topside Martian ionosphere, as reported in section 3, is likely persistent for the entire range of SZA from subsolar to near terminator.

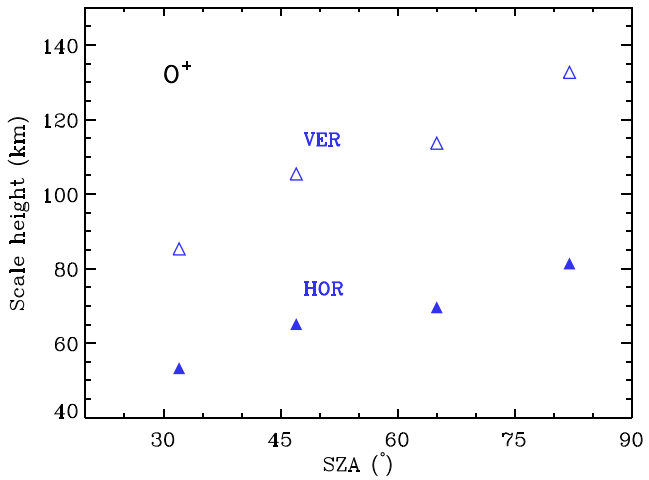


**Figure 11.** The topside $O^+$ density scale heights for regions with near-vertical (VER) and near-horizontal (HOR) field lines, both as a function of SZA on the dayside of Mars. The drawing convention is the same as in Figures 4 and 5.

On the nightside of Mars for which Figure 9 reveals a considerably larger ionospheric variability than on the dayside, the interpretation of the ion density scale heights derived from the median density profiles in sections 2 and 3 is more complicated. In some cases, the appropriate ion density scale heights cannot be rigorously determined as the ion densities do not decay near exponentially with increasing altitude. The nightside defined in the present study is restricted to SZA >120° where day-to-night plasma transport is negligible and surpassed by SW electron precipitation (e.g., Cui et al., 2015; Němec et al., 2010; Withers et al., 2012). As a consequence, the nightside ionosphere is patchy and closely modulated by the ambient magnetic field configuration (e.g., Lillis & Brain, 2013; Lillis & Fang, 2015; Lillis et al., 2009, 2011, 2018). Recently, Xu, Mitchell, Liemohn, et al. (2017) obtained the magnetic topology mappings on both the dayside and the nightside of Mars with the aid of the electron pitch angle distribution measured by the MAVEN Solar Wind Electron Analyzer. At 300–500 km, the nightside regions away from strong crustal anomalies are dominated by (near-horizontal) draped field lines to which SW electrons have direct access, providing a source of ionization. In contrast, the nightside regions over crustal anomalies, characterized by near-vertical field lines according to Figure 3, are

populated with suprathermal electron voids indicating that a local source of ionization is in general absent (see also Steckiewicz et al., 2015, 2017). Despite this, a reduced ionosphere is in practice observable within these regions (see Figure 5) from which an ion density scale height can be derived for each species. This is likely connected to the nonvanishing probabilities for the occurrences of draped and open field lines, especially above 400 km (see Figures 9 and 10 of Xu, Mitchell, Liemohn, et al., 2017), but these field lines are by no means a common feature. Accordingly, the topside ion density scale heights reported in sections 2 and 3 are representative of the common behavior of the nightside Martian ionosphere for regions with near-horizontal field lines but not necessarily for regions with near-vertical field lines.

For regions of the topside Martian ionosphere with near-horizontal field lines, a detailed evaluation of the ion force balance is performed in the vertical direction. Our analysis indicates that, for the dayside ions, the dominant force is provided by magnetic pressure above 330 km and by ambipolar electric field at lower altitudes. For the nightside ions, the force balance is almost exclusively contributed by magnetic pressure due to the substantial depletion of the Martian ionosphere in darkness (e.g., Girazian, Mahaffy, Lillis, Benna, Elrod, Jakosky, et al., 2017; Girazian, Mahaffy, Lillis, Benna, Elrod, Fowler, et al., 2017). On both sides, the total force per ion is nearly common to all species at any given altitude. Since the total force is always upward orientated, bulk ion outflow is expected on both the dayside and the nightside of Mars. Specifically, the dayside ion outflow that we find based on the MAVEN NGIMS data confirms the early conclusion drawn from the Viking RPA data (e.g., Chen et al., 1978; Fox, 1997, 2009; Kar et al., 1996).

At a reference altitude of 500 km, the typical ion outflow velocity is predicted to be ~4 km/s on the dayside and ~20 km/s on the nightside, with respective Mach numbers of around 3.3 and 14 indicative of supersonic ion outflow at high altitudes. On the dayside, the corresponding ion outward fluxes range from $2.4 \times 10^7$ and $1.6 \times 10^7$ cm$^{-2}$ s$^{-1}$ for $O_2^+$ and $O^+$ as the two most abundant species in the topside Martian ionosphere (e.g., Benna, Mahaffy, Grebowsky, Fox, et al., 2015) down to several $10^5$ cm$^{-2}$ s$^{-1}$ for minor species such as $CO_2^+$ and $OCOH^+$, in response to the density variability among different species. On the nightside, the ion outward fluxes of the species considered here are comparable, at the level of $10^6$ cm$^{-2}$ s$^{-1}$. The dayside and nightside total ion outward fluxes are $5.0 \times 10^7$ and $1.3 \times 10^7$ cm$^{-2}$ s$^{-1}$ at 500 km. The respective ion outflow rates are $4.8 \times 10^{25}$ s$^{-1}$ on the dayside and $1.2 \times 10^{25}$ s$^{-1}$ on the nightside, both evaluated with a hemispheric surface area at 500 km on Mars. We emphasize that the nightside ion outward flux and outflow rate quoted above should be taken with caution because we implicitly assume that these values, while derived for the deep nightside of Mars with the ionosphere mainly produced by electron precipitation, also represent roughly the situation for the cross-terminator regions with the ionosphere mainly contributed by day-to-night plasma transport. The actual situation is more likely manifest as a steady decrease in ion outfward flux across the terminator, but this should not have a significant impact on the derived total ion escape rate (see below) since the boundary between the dayside and the nightside defined in this study has a relatively small contribution to the total surface area at 500 km on Mars. In terms of the diurnal difference in outward flux or outflow rate, we note that the nightside depletion in total ion density by a factor of around 40 as compared to the dayside is substantially reduced by the nightside enhancement in ion flow velocity by a factor of more than 4.

It would be instructive to compare the dayside ion fluxes obtained in this study to those of Fox (2009). The latter work predicted a dayside upward $O_2^+$ flux of $5 \times 10^7$ cm$^{-2}$ s$^{-1}$ and a dayside upward $O^+$ flux of $4 \times 10^6$ cm$^{-2}$ s$^{-1}$, both appropriate for the solar minimum conditions. The flux that we predict is about a factor of 2 lower for $O_2^+$ but a factor of 4 higher for $O^+$. These differences could be partially attributed to the different conditions of solar activity involved, but two caveats ought to be emphasized. First, the Fox (2009) model assumes diffusion approximation for which the bulk ion outflow is controlled by the ion-neutral collisions at altitudes up to 400 km, whereas in our work, such an approximation is shown to fail at sufficiently low altitudes down to at least 300 km, and the ion outflow velocity is obtained instead with the high-altitude approximation of Cravens et al. (2017) in the supersonic flow regime. Second, the contribution of magnetic pressure to the ion force balance is neglected in Fox (2009) but is shown here to be dominant over the other force terms above 330 km. In fact, these two caveats are closely related because without magnetic pressure, the ions cannot be accelerated to supersonic and the diffusion approximation becomes valid.

The dayside ion outflow implied by the MAVEN data either helps to maintain a substantial nightside ionosphere on Mars (e.g., Brain et al., 2015; Cui et al., 2015; Girazian, Mahaffy, Lillis, Benna, Elrod, Jakosky, et al., 2017; Němec et al., 2010; Withers et al., 2012) or leads to considerable plasma escape down the tail (e.g., Barabash et al., 2007; Dubinin, Fraenz, Pätzold, McFadden, et al., 2017; Dubinin, Fraenz, Pätzold,

Andrews, et al., 2017; Edberg et al., 2010; Lundin et al., 2013; Ramstad et al., 2015). The relative contributions of these two channels are comparable as predicted by existing magnetohydrodynamic calculations (e.g., Ma et al., 2004). For instance, the cross-terminator cold ion flow rate was estimated to be $\sim 3 \times 10^{25}$ $s^{-1}$ based on the MEx Analyzer of Space Plasmas and Energetic Atoms 3 measurements (e.g., Fränz et al., 2010), which should represent the combined effect of day-to-night transport and escape. It is also interesting to note that in order to interpret the observed cross-terminator depletion of total electron content measured by the MEx MARSIS at the dusk side of the Martian ionosphere, Cui et al. (2015) obtained a large ion transport velocity of 2 km/s,which is compatible with the dayside ion outflow velocity listed in Table 1 and supports our conjecture of a portion of the dayside ions ultimately flowing to the nightside. Accordingly, we estimate a total ion escape rate on Mars to be $\sim 3.6 \times 10^{25}$ $s^{-1}$, which is the combination of half of the ion outflow on the dayside and the entire ion outflow on the nightside. Here we have implicitly assumed that the nightside ion outflow rate estimated from the MAVEN data appropriately represents the nightside ion escape rate.

Based on the calculations performed in this study, we cannot draw firm conclusions on the characteristics of bulk ion flow for regions with near-vertical field lines which could then be compared with those inferred for regions with near-horizontal field lines (see section 4). On the dayside, vertical field lines allow efficient ion transport in the vertical direction (Matta et al., 2015), which naturally leads to a more extended ion distribution as implied by the NGIMS OSI data. Interestingly, Lundin et al. (2011) reported the observation of enhanced dayside $O^+$ outward flux near strong crustal anomalies, appropriate for the energy range from 10 up to 200 eV. This is higher than the typical energy of NGIMS sampled cold ions at the level of 0.1 eV, and it remains to be seen how the pattern of cold ion dynamics comes out via a future evaluation of the ion force balance over regions with near-vertical field lines. On the nightside, the opposite observation of the impact of magnetic field configuration is likely related to the dominance of draped field lines away from strong crustal anomalies, to be compared with the rare occurrence of these field lines near crustal anomalies (Xu, Mitchell, Liemohn, et al., 2017).

Finally, we end this section with a discussion of the uncertainties in the MAVEN-based results presented so far. The uncertainties in the topside ion density scale height are quite small, typically at the level of 1 km, since the ion density profiles shown here are the median results obtained from many orbits. The ion force balance inferred from the data is also robust due to the dominant role of magnetic pressure, along with the accurate measurement of the magnetic field by the magnetometer (Connerney et al., 2015). One important uncertainty in the derived ion flow velocities is related to the use of equation (2). In reaching this equation, we assume that the flow velocity at the bottom boundary of 180 km is much smaller than the velocity at the top boundary of 500 km and that the column integrated contribution from ion-neutral collisions is also negligible. The uncertainty due to the former approximation should be tiny since the ion flow velocities at 180 km are well below 0.1 km/s estimated with the diffusion approximation. The uncertainty due to the latter approximation should not exceed 5%, estimated from the integration of the ion-neutral collision term, $m_i \nu_{in} W_i$ (see equation (A8)), over the altitude range of 180–500 km where $W_i$ is taken from the solution under high-altitude approximation. We caution that other approximations inherent in equations (1) and (2), such as the neglect of the vertical magnetic field component and the application of a common ion velocity profile to all species involved, may also introduce additional uncertainties to the derived ion outflow velocities.

## 6. Concluding Remarks

Prior to the MAVEN mission, the only information on the composition of the Martian ionosphere came from the Viking RPA data (Hanson et al., 1977), which revealed the presence of substantial ion outflow on the dayside of Mars (e.g., Chen et al., 1978; Fox, 1997, 2009; Kar et al., 1996). The extensive measurements made by the MAVEN NGIMS allow us to examine the morphology of the topside Martian ionosphere not only in unprecedented detail but also on both the dayside and the nightside of the planet (e.g., Benna, Mahaffy, Grebowsky, Fox, et al., 2015; Girazian, Mahaffy, Lillis, Benna, Elrod, Jakosky, et al., 2017; Girazian, Mahaffy, Lillis, Benna, Elrod, Fowler, et al., 2017).

Above 300 km in the Martian ionosphere, various species present a more or less constant density scale height around 100 km with a variability of 10% on the dayside and around 180 km with a variability of 6% on the nightside. The data also reveal a prominent variation with magnetic field orientation in that the ion distribution over regions with near-vertical field lines tends to be more extended on the dayside but more

concentrated on the nightside, respectively. Combining these observations should have important implications on the pattern of ion dynamics in the vicinity of Mars. Via an analysis of the observed ionospheric variability, we argue that the dayside median observations are quite representative of the common dayside behavior irrespective of SZA, over regions with both near-vertical and near-horizontal field lines, whereas the nightside median observations reported here reflect the common nightside behavior over regions with near-horizontal field lines but not necessarily over regions with near-vertical field lines.

With the aid of the data acquired by several other instruments onboard MAVEN, a detailed evaluation of the ion force balance is performed, highlighting the importance of magnetic pressure on both the dayside and the nightside of Mars. Such an analysis, appropriate for regions with near-horizontal field lines, suggests the presence of strong bulk ion outflow across the entire surface of Mars. At a reference altitude of 500 km, the characteristic ion outflow velocities are predicted to be 4 km/s on the dayside and 20 km/s on the nightside. The corresponding Mach numbers are around 3.3 and 14, respectively, implying that the ion outflow is highly supersonic, compatible with the high-altitude approximation of Cravens et al. (2017). We estimate the total ion outflow rates to be $4.8 \times 10^{25}$ s$^{-1}$ on the dayside and $1.2 \times 10^{25}$ s$^{-1}$ on the nightside, of which the former may represent the combination of day-to-night plasma transport (e.g., Brain et al., 2015; Cui et al., 2015; Girazian, Mahaffy, Lillis, Benna, Elrod, Jakosky, et al., 2017; Němec et al., 2010; Withers et al., 2012) and ion escape down the tail (e.g., Barabash et al., 2007; Dubinin, Fraenz, Pätzold, McFadden, et al., 2017; Dubinin, Fraenz, Pätzold, Andrews, et al., 2017; Edberg et al., 2010; Lundin et al., 2013; Ramstad et al., 2015).

## Appendix A: Derivation of the Ion Momentum Equation

Following Matta et al. (2015), we write the steady state ion momentum equation for a given species, i, of the Martian ionosphere as

$$\vec{V}_\mathrm{i} \cdot \vec{\nabla}\vec{V}_\mathrm{i} + \frac{1}{m_\mathrm{i} n_\mathrm{i}} \vec{\nabla}(n_\mathrm{i} k T_\mathrm{i}) - \vec{g} - \frac{e}{m_\mathrm{i}}(\vec{E} + \frac{1}{c}\vec{V}_\mathrm{i} \times \vec{B}) + \nu_\mathrm{in}\vec{V}_\mathrm{i} = 0, \tag{A1}$$

and similarly we write the steady state electron momentum equation as

$$\frac{1}{m_\mathrm{e} n_\mathrm{e}} \vec{\nabla}(n_\mathrm{e} k T_\mathrm{e}) + \frac{e}{m_\mathrm{e}}(\vec{E} + \frac{1}{c}\vec{V}_\mathrm{e} \times \vec{B}) = 0, \tag{A2}$$

where $n_\mathrm{i}$ and $n_\mathrm{e}$ are the ion and electron number densities, $T_\mathrm{i}$ and $T_\mathrm{e}$ are the ion and electron temperatures, $V_\mathrm{i}$ and $V_\mathrm{e}$ are the ion and electron flow velocities, $\vec{E}$ and $\vec{B}$ are the electric and magnetic fields, $\vec{g}$ is the local gravity, $k$ is the Boltzmann constant, $e$ is the electric charge, and $\nu_\mathrm{in}$ is the total ion-neutral momentum transfer collision frequency. Several approximations are implicitly used in reaching the above equation including (1) a stationary neutral background atmosphere, (2) a common temperature profile for all ion species, (3) a common flow velocity profile for all ion species which implies that all Coulomb interaction terms, proportional to the relative ion velocities, can be ignored, (4) negligible contributions to the electron momentum equation due to all force terms proportional to the electron mass, and (5) persistently subsonic electron flow due to the very large electron-acoustic velocity typically around 200 km/s in the topside Martian ionosphere. Combining equations (A1) and (A2) to eliminate the electric field term, we have

$$\vec{V}_\mathrm{i} \cdot \vec{\nabla}\vec{V}_\mathrm{i} + \frac{1}{m_\mathrm{i} n_\mathrm{i}} \vec{\nabla}(n_\mathrm{i} k T_\mathrm{i}) + \frac{1}{m_\mathrm{i} n_\mathrm{e}} \vec{\nabla}(n_\mathrm{e} k T_\mathrm{e}) - \vec{g} - \frac{e}{m_\mathrm{i} c}(\vec{V}_\mathrm{i} - \vec{V}_\mathrm{e}) \times \vec{B} + \nu_\mathrm{in}\vec{V}_\mathrm{i} = 0, \tag{A3}$$

with the $z$-component written as

$$W_\mathrm{i}\frac{\mathrm{d}W_\mathrm{i}}{\mathrm{d}z} + \frac{1}{m_\mathrm{i} n_\mathrm{i}}\frac{\mathrm{d}(n_\mathrm{i} k T_\mathrm{i})}{\mathrm{d}z} + \frac{1}{m_\mathrm{i} n_\mathrm{e}}\frac{\mathrm{d}(n_\mathrm{e} k T_\mathrm{e})}{\mathrm{d}z} + g - \frac{e}{m_\mathrm{i} c}[(U_\mathrm{i} - U_\mathrm{e})B_y - (V_\mathrm{i} - V_\mathrm{e})B_x)] + \nu_\mathrm{in} W_\mathrm{i} = 0, \tag{A4}$$

where $U_\mathrm{i}$ ($U_\mathrm{e}$), $V_\mathrm{i}$ ($V_\mathrm{e}$), and $W_\mathrm{i}$ ($W_\mathrm{e}$) are the $x$, $y$, and $z$ components of the ion (electron) flow velocity, and we have also implicitly ignored the horizontal variations of $W_\mathrm{i}$ (see below for the definition of the coordinate system used).

According to Ampére's law, the ion and electron flow velocities are related to the magnetic field via

$$\vec{\nabla} \times \vec{B} = \frac{4\pi e n_\mathrm{e}}{c}(\vec{V}_\mathrm{i} - \vec{V}_\mathrm{e}), \tag{A5}$$

where $c$ is the speed of light and the right-hand side is proportional to the electric current, $\vec{J}$, given by $\vec{J} = e n_\mathrm{e}(\vec{V}_\mathrm{i} - \vec{V}_\mathrm{e})$. For simplicity, we assume that the magnetic field, $\vec{B}$, in the topside Martian ionosphere is purely

horizontal with $\vec{B} = B_x(x, y, z)\hat{x} + B_y(x, y, z)\hat{y}$, where $\hat{x}$, $\hat{y}$, and $\hat{z}$ are the unit vectors in a locally defined coordinate system with positive $x$ pointing to east, positive $y$ pointing to north, and positive $z$ pointing to vertically upward, respectively. Based on existing observations (e.g., Akalin et al., 2010; Brain et al., 2006; Connerney et al., 2015; Mitchell et al., 2001; Xu, Mitchell, Liemohn, et al., 2017) and model calculations (e.g., Ma et al., 2002, 2004, 2014), the above expression reasonably describes the magnetic field topology in the vicinity of Mars except for restricted regions near strong crustal magnetic anomalies. Then the $x$ and $y$ components of equation (A5) become

$$\frac{4\pi e n_e}{c}(U_i - U_e) = -\frac{dB_y}{dz}, \tag{A6}$$

and

$$\frac{4\pi e n_e}{c}(V_i - V_e) = \frac{dB_x}{dz}, \tag{A7}$$

from which equation (A4) can be recast as

$$W_i\frac{dW_i}{dz} + \frac{1}{m_i n_i}\frac{d(n_i k T_i)}{dz} + \frac{1}{m_i n_e}\frac{d(n_e k T_e)}{dz} + g + \frac{1}{m_i n_e}\frac{d}{dz}\left(\frac{B_h^2}{8\pi}\right) + \nu_{in} W_i = 0, \tag{A8}$$

where $B_h = \sqrt{B_x^2 + B_y^2}$ is the horizontal magnetic field strength. Equation (A8) is used in section 4 to evaluate the force balance for each species as well as to estimate the respective ion flow velocity in the topside Martian ionosphere characterized by large-scale draped magnetic fields.

**Acknowledgments**

J. C. and Y. W. acknowledge support from the National Natural Science Foundation of China (grants 41525015, 41774186, and 41525016). J. C. is also supported by the Science and Technology Development Fund of Macau SAR (039/2013/A2 and 119/2017/A3). S. X. thanks the National Aeronautics and Space Administration (NASA) supporting the MAVEN project through the Mars Exploration Program. E. V. is grateful for funding from the Swedish National Space Agency (contract 166/14). N. J. T. E. acknowledges funding from the Swedish National Space Agency (135/13) and the Swedish Research Council (VR grant 621-2013-4191). The data used in the present study are publicly available at the MAVEN Science Data Center (https://lasp.colorado.edu/maven/sdc/public/). We appreciate the two anonymous reviewers for their constructive comments, which have significantly improved the quality of the manuscript.

## References

Acuna, M. H., Connerney, J. E. P., Ness, N. F., Lin, R. P., Mitchell, D., Carlson, C. W., et al. (1999). Global distribution of crustal magnetization discovered by the Mars global surveyor MAG/ER experiment. *Science*, *284*, 790.

Acuna, M. H., Connerney, J. E. P., Wasilewski, P., Lin, R. P., Anderson, K. A., Carlson, C. W., et al. (1998). Magnetic field and plasma observations at Mars: Initial results of the Mars Global Surveyor Mission. *Science*, *279*, 1676–1680.

Akalin, F., Morgan, D. D., Gurnett, D. A., Kirchner, D. L., Brain, D. A., Modolo, R., et al. (2010). Dayside induced magnetic field in the ionosphere of Mars. *Icarus*, *206*, 104–111.

Andersson, L., Ergun, R. E., Delory, G. T., Eriksson, A., Westfall, J., Reed, H., et al. (2015). The Langmuir probe and waves (LPW) instrument for MAVEN. *Space Science Reviews*, *195*, 173–198.

Andrews, D. J., André, M., Opgenoorth, H. J., Edberg, N. J. T., Diéval, C., Duru, F., et al. (2014). Oblique reflections in the Mars Express MARSIS data set: Stable density structures in the Martian ionosphere. *Journal of Geophysical Research: Space Physics*, *119*, 3944–3960. https://doi.org/10.1002/2013JA019697

Andrews, D. J., Edberg, N. J. T., Eriksson, A. I., Gurnett, D. A., Morgan, D., Němec, F., & Opgenoorth, H. J. (2015). Control of the topside Martian ionosphere by crustal magnetic fields. *Journal of Geophysical Research: Space Physics*, *120*, 3042–3058. https://doi.org/10.1002/2014JA020703

Barabash, S., Fedorov, A., Lundin, R., & Sauvaud, J.-A. (2007). Martian atmospheric erosion rates. *Science*, *315*, 501–503.

Benna, M., Mahaffy, P. R., Grebowsky, J. M., Fox, J. L., Yelle, R. V., & Jakosky, B. M. (2015). First measurements of composition and dynamics of the Martian ionosphere by MAVEN's Neutral Gas and Ion Mass Spectrometer. *Geophysical Research Letters*, *42*, 8958–8965. https://doi.org/10.1002/2015GL066146

Benna, M., Mahaffy, P. R., Grebowsky, J. M., Plane, J. M. C., Yelle, R. V., & Jakosky, B. M. (2015). Metallic ions in the upper atmosphere of Mars from the passage of comet C/2013 A1 (Siding Spring). *Geophysical Research Letters*, *42*, 4670–4675. https://doi.org/10.1002/2015GL064159

Brain, D. A., McFadden, J. P., Halekas, J. S., Connerney, J. E. P., Bougher, S. W., Curry, S., et al. (2015). The spatial distribution of planetary ion fluxes near Mars observed by MAVEN. *Geophysical Research Letters*, *42*, 9142–9148. https://doi.org/10.1002/2015GL065293

Brain, D. A., Mitchell, D. L., & Halekas, J. S. (2006). The magnetic field draping direction at Mars from April 1999 through August 2004. *Icarus*, *182*, 464–473.

Chen, R. H., Cravens, T. E., & Nagy, A. F. (1978). The Martian ionosphere in light of the Viking observations. *Journal of Geophysical Research*, *83*, 3871–3876.

Choi, Y. W., Kim, J., Min, K. W., Nagy, A. F., & Oyama, K. I. (1998). Effect of the magnetic field on the energetics of Mars ionosphere. *Geophysical Research Letters*, *25*, 2753–2756.

Comfort, R. H. (1988). *The magnetic mirror force in plasma fluid models, Monograph Series* (Vol. 44, p. 51). Washington, DC: American Geophysical Union Geophysical.

Connerney, J. E. P., Acuna, M. H., Wasilewski, P. J., Ness, N. F., Reme, H., Mazelle, C., et al. (1999). Magnetic lineations in the ancient crust of Mars. *Science*, *284*, 794.

Connerney, J. E. P., Espley, J. R., DiBraccio, G. A., Gruesbeck, J. R., Oliversen, R. J., Mitchell, D. L., et al. (2015). First results of the MAVEN magnetic field investigation. *Geophysical Research Letters*, *42*, 8819–8827. https://doi.org/10.1002/2015GL065366

Cravens, T. E., Hamil, O., Houston, S., Bougher, S., Ma, Y., Brain, D., & Ledvina, S. (2017). Estimates of ionospheric transport and ion loss at Mars. *Journal of Geophysical Research: Space Physics*, *122*, 10,626–10,637. https://doi.org/10.1002/2017JA024582

Cravens, T. E., Shinagawa, H., & Nagy, A. F. (1984). The evolution of large-scale magnetic fields in the ionosphere of Venus. *Geophysical Research Letters*, *11*, 267–270.

Cui, J., Galand, M., Yelle, R. V., Wahlund, J.-E., Ågren, K., Waite, J. H., & Dougherty, M. K. (2010). Ion transport in Titan's upper atmosphere. *Journal of Geophysical Research*, *115*, A06314. https://doi.org/10.1029/2009JA014563

Cui, J., Galand, M., Yelle, R. V., Wei, Y., & Zhang, S.-J. (2015). Day-to-night transport in the Martian ionosphere: Implications from total electron content measurements. *Journal of Geophysical Research: Space Physics*, *120*, 2333–2346. https://doi.org/10.1002/2014JA020788

Cui, J., Yelle, R. V., Zhao, L.-L., Stone, S., Jiang, F.-Y., Cao, Y.-T., et al. (2018). The impact of crustal magnetic fields on the thermal structure of the Martian upper atmosphere. *Astrophysical Journal Letters*, *853*, L33.

Diéval, C., Andrews, D. J., Morgan, D. D., Brain, D. A., & Gurnett, D. A. (2015). MARSIS remote sounding of localized density structures in the dayside Martian ionosphere: A study of controlling parameters. *Journal of Geophysical Research: Space Physics*, *120*, 8125–8145. https://doi.org/10.1002/2015JA021486

Diéval, C., Kopf, A. J., & Wild, J. A. (2018). Shapes of magnetically controlled electron density structures in the dayside Martian ionosphere. *Journal of Geophysical Research: Space Physics*, *123*, 3919–3942. https://doi.org/10.1002/2017JA025140

Dubinin, E., Fraenz, M., Pätzold, M., Andrews, D., Vaisberg, O., Zelenyi, L., & Barabash, S. (2017). Martian ionosphere observed by Mars Express. 2. Influence of solar irradiance on upper ionosphere and escape fluxes. *Planetary and Space Science*, *145*, 1–8.

Dubinin, E., Fraenz, M., Pätzold, M., McFadden, J., Halekas, J. S., DiBraccio, G. A., et al. (2017). The effect of solar wind variations on the escape of oxygen ions from Mars through different channels: MAVEN observations. *Journal of Geophysical Research: Space Physics*, *122*, 11,285–11,301. https://doi.org/10.1002/2017JA024741

Duru, F., Gurnett, D. A., Averkamp, T. F., Kirchner, D. L., Huff, R. L., Persoon, A. M., et al. (2006). Magnetically controlled structures in the ionosphere of Mars. *Journal of Geophysical Research*, *111*, A12204. https://doi.org/10.1029/2006JA011975

Duru, F., Gurnett, D. A., Morgan, D. D., Modolo, R., Nagy, A. F., & Najib, D. (2008). Electron densities in the upper ionosphere of Mars from the excitation of electron plasma oscillations. *Journal of Geophysical Research*, *113*, A07302. https://doi.org/10.1029/2008JA013073

Edberg, N. J. T., Lester, M., Cowley, S. W. H., & Eriksson, A. I. (2008). Statistical analysis of the location of the Martian magnetic pileup boundary and bow shock and the influence of crustal magnetic fields. *Journal of Geophysical Research*, *113*, A08206. https://doi.org/10.1029/2008JA013096

Edberg, N. J. T., Nilsson, H., Williams, A. O., Lester, M., Milan, S. E., Cowley, S. W. H., et al. (2010). Pumping out the atmosphere of Mars through solar wind pressure pulses. *Geophysical Research Letters*, *37*, L03107. https://doi.org/10.1029/2009GL041814

Ergun, R. E., Andersson, L. A., Fowler, C. M., Woodson, A. K., Weber, T. D., Delory, G. T., et al. (2016). Enhanced $O_2^+$ loss at Mars due to an ambipolar electric field from electron heating. *Journal of Geophysical Research: Space Physics*, *121*, 4668–4678. https://doi.org/10.1002/2016JA022349

Fox, J. L. (1997). Upper limits to the outflow of ions at Mars: Implications for atmospheric evolution. *Geophysical Research Letters*, *24*, 2901. https://doi.org/10.1029/97GL52842

Fox, J. L. (2003). Effect of $H_2$ on the Martian ionosphere: Implications for atmospheric evolution. *Journal of Geophysical Research*, *108*(A6), 1223. https://doi.org/10.1029/2001JA000203

Fox, J. L. (2004). Response of the Martian thermosphere/ionosphere to enhanced fluxes of solar soft X rays. *Journal of Geophysical Research*, *109*, A11310. https://doi.org/10.1029/2004JA010380

Fox, J. L. (2009). Near-terminator Venus ionosphere: How Chapman-esque? *Journal of Geophysical Research*, *114*, E12005. https://doi.org/10.1029/2006JE002736

Fox, J. L., Benna, M., Mahaffy, P. R., & Jakosky, B. M. (2015). Water and water ions in the Martian thermosphere/ionosphere. *Geophysical Research Letters*, *42*, 8977–8985. https://doi.org/10.1002/2015GL065465

Fox, J. L., & Weber, A. J. (2012). MGS electron density profiles: Analysis and modeling of peak altitudes. *Icarus*, *221*, 1002–1019.

Fox, J. L., & Yeager, K. E. (2006). Morphology of the near-terminator Martian ionosphere: A comparison of models and data. *Journal of Geophysical Research*, *111*, A10309. https://doi.org/10.1029/2006JA011697

Fox, J. L., & Yeager, K. E. (2009). MGS electron density profiles: Analysis of the peak magnitudes. *Icarus*, *200*, 468–479.

Fränz, M., Dubinin, E., Nielsen, E., Woch, J., Barabash, S., Lundin, R., & Fedorov, A. (2010). Transterminator ion flow in the Martian ionosphere. *Planetary and Space Science*, *58*, 1442–1454.

Girazian, Z., Mahaffy, P., Lillis, R. J., Benna, M., Elrod, M., Fowler, C. M., & Mitchell, D. L. (2017). Ion densities in the nightside ionosphere of Mars: Effects of electron impact ionization. *Geophysical Research Letters*, *44*, 11,248–11,256. https://doi.org/10.1002/2017GL075431

Girazian, Z., Mahaffy, P. R., Lillis, R. J., Benna, M., Elrod, M., & Jakosky, B. M. (2017). Nightside ionosphere of Mars: Composition, vertical structure, and variability. *Journal of Geophysical Research: Space Physics*, *122*, 4712–4725. https://doi.org/10.1002/2016JA023508

González-Galindo, F., Chaufray, J.-Y., López-Valverde, M. A., Gilli, G., Forget, F., Leblanc, F., et al. (2013). Three-dimensional Martian ionosphere model: I. The photochemical ionosphere below 180 km. *Journal of Geophysical Research: Planets*, *118*, 2105–2123. https://doi.org/10.1002/jgre.20150

Gurnett, D. A., Huff, R. L., Morgan, D. D., Persoon, A. M., Averkamp, T. F., Kirchner, D. L., et al. (2008). An overview of radar soundings of the martian ionosphere from the Mars Express spacecraft. *Advances in Space Research*, *41*, 1335–1346.

Gurnett, D. A., Kirchner, D. L., Huff, R. L., Morgan, D. D., Persoon, A. M., Averkamp, T. F., et al. (2005). Radar soundings of the ionosphere of Mars. *Science*, *310*, 1929–1933.

Hanson, W. B., Sanatani, S., & Zuccaro, D. R. (1977). The Martian ionosphere as observed by the Viking retarding potential analyzers. *Journal of Geophysical Research*, *82*, 4351–4363.

Harada, Y., Halekas, J. S., DiBraccio, G. A., Xu, S., Espley, J., Mcfadden, J. P., et al. (2018). Magnetic reconnection on dayside crustal magnetic fields at Mars: MAVEN observations. *Geophysical Research Letters*, *45*, 4550–4558. https://doi.org/10.1002/2018GL077281

Jakosky, B. M., Grebowsky, J. M., Luhmann, J. G., & Brain, D. A. (2015). Initial results from the MAVEN mission to Mars. *Geophysical Research Letters*, *42*, 8791–8802. https://doi.org/10.1002/2015GL065271

Kar, J., Mahajan, K. K., & Kohli, R. (1996). On the outflow of $O_2^+$ ions at Mars. *Journal of Geophysical Research*, *101*, 12,747–12,752.

Langlais, B., Purucker, M. E., & Mandea, M. (2004). Crustal magnetic field of Mars. *Journal of Geophysical Research*, *109*, E02008. https://doi.org/10.1029/2003JE002048

Lillis, R. J., & Brain, D. A. (2013). Nightside electron precipitation at Mars: Geographic variability and dependence on solar wind conditions. *Journal of Geophysical Research: Space Physics*, *118*, 3546–3556. https://doi.org/10.1002/jgra.50171

Lillis, R. J., & Fang, X. (2015). Electron impact ionization in the Martian atmosphere: Interplay between scattering and crustal magnetic field effects. *Journal of Geophysical Research: Planets*, *120*, 1332–1345. https://doi.org/10.1002/2015JE004841

Lillis, R. J., Fillingim, M. O., & Brain, D. A. (2011). Three-dimensional structure of the Martian nightside ionosphere: Predicted rates of impact ionization from Mars Global Surveyor magnetometer and electron reflectometer measurements of precipitating electrons. *Journal of Geophysical Research*, *116*, A12317. https://doi.org/10.1029/2011JA016982

Lillis, R. J., Fillingim, M. O., Peticolas, L. M., Brain, D. A., Lin, R. P., & Bougher, S. W. (2009). Nightside ionosphere of Mars: Modeling the effects of crustal magnetic fields and electron pitch angle distributions on electron impact ionization. *Journal of Geophysical Research*, *114*, E11009. https://doi.org/10.1029/2009JE003379

Lillis, R. J., Mitchell, D. L., Lin, R. P., Connerney, J. E. P., & Acuña, M. H. (2004). Mapping crustal magnetic fields at Mars using electron reflectometry. *Geophysical Research Letters*, *31*, L15702. https://doi.org/10.1029/2004GL020189

Lillis, R. J., Mitchell, D. L., Steckiewicz, M., Brain, D., Xu, S., Weber, T., et al. (2018). Ionizing electrons on the Martian nightside: Structure and variability. *Journal of Geophysical Research: Space Physics*, *123*, 4349–4363. https://doi.org/10.1029/2017JA025151

Luhmann, J. G., Russell, C. T., & Elphic, R. C. (1984). Time scales for the decay of induced large-scale magnetic fields in the Venus ionosphere. *Journal of Geophysical Research*, *89*, 362–368.

Lundin, R., Barabash, S., Holmström, M., Nilsson, H., Futaana, Y., Ramstad, R., et al. (2013). Solar cycle effects on the ion escape from Mars. *Geophysical Research Letters*, *40*, 6028–6032. https://doi.org/10.1002/2013GL058154

Lundin, R., Barabash, S., Yamauchi, M., Nilsson, H., & Brain, D. (2011). On the relation between plasma escape and the Martian crustal magnetic field. *Geophysical Research Letters*, *38*, L02102. https://doi.org/10.1029/2010GL046019

Ma, Y., Fang, X., Russell, C. T., Nagy, A. F., Toth, G., Luhmann, J. G., et al. (2014). Effects of crustal field rotation on the solar wind plasma interaction with Mars. *Geophysical Research Letters*, *41*, 6563–6569. https://doi.org/10.1002/2014GL060785

Ma, Y., Nagy, A. F., Hansen, K. C., Dezeeuw, D. L., Gombosi, T. I., & Powell, K. G. (2002). Three-dimensional multispecies MHD studies of the solar wind interaction with Mars in the presence of crustal fields. *Journal of Geophysical Research*, *107*(A10), 1282. https://doi.org/10.1029/2002JA009293

Ma, Y., Nagy, A. F., Sokolov, I. V., & Hansen, K. C. (2004). Three-dimensional, multispecies, high spatial resolution MHD studies of the solar wind interaction with Mars. *Journal of Geophysical Research*, *109*, A07211. https://doi.org/10.1029/2003JA010367

Mahaffy, P. R., Benna, M., Elrod, M., Yelle, R. V., Bougher, S. W., Stone, S. W., & Jakosky, B. M. (2015). Structure and composition of the neutral upper atmosphere of Mars from the MAVEN NGIMS investigation. *Geophysical Research Letters*, *42*, 8951–8957. https://doi.org/10.1002/2015GL065329

Mahaffy, P. R., Benna, M., King, T., Harpold, D. N., Arvey, R., Barciniak, M., et al. (2015). The neutral gas and ion mass spectrometer on the Mars atmosphere and volatile evolution mission. *Space Science Reviews*, *195*, 49–73.

Martinis, C. R., Wilson, J. K., & Mendillo, M. J. (2003). Modeling day-to-day ionospheric variability on Mars. *Journal of Geophysical Research*, *108*(A10), 1383. https://doi.org/10.1029/2003JA009973

Matta, M., Mendillo, M., Withers, P., & Morgan, D. (2015). Citation for: Interpreting Mars ionospheric anomalies over crustal magnetic field regions using a 2-D ionospheric model. *Journal of Geophysical Research: Space Physics*, *120*, 766–777. https://doi.org/10.1002/2014JA020721

Matta, M., Withers, P., & Mendillo, M. (2013). The composition of Mars' topside ionosphere: Effects of hydrogen. *Journal of Geophysical Research: Space Physics*, *118*, 2681–2693. https://doi.org/10.1002/jgra.50104

McFadden, J. P., Kortmann, O., Curtis, D., Dalton, G., Johnson, G., Abiad, R., et al. (2015). MAVEN SupraThermal and Thermal Ion Compostion (STATIC) instrument. *Space Science Reviews*, *195*, 199–256.

Mendillo, M., Marusiak, A. G., Withers, P., Morgan, D., & Gurnett, D. (2013). A new semiempirical model of the peak electron density of the Martian ionosphere. *Geophysical Research Letters*, *40*, 5361–5365. https://doi.org/10.1002/2013GL057631

Mendillo, M., Narvaez, C., Matta, M., Vogt, M., Mahaffy, P., Benna, M., & Jakosky, B. (2015). MAVEN and the Mars initial reference ionosphere model. *Geophysical Research Letters*, *42*, 9080–9086. https://doi.org/10.1002/2015GL065732

Mendillo, M., Narvaez, C., Vogt, M. F., Mayyasi, M., Forbes, J., Galand, M., et al. (2017). Sources of ionospheric variability at Mars. *Journal of Geophysical Research: Space Physics*, *122*, 9670–9684. https://doi.org/10.1002/2017JA024366

Mitchell, D. L., Lin, R. P., Mazelle, C., Reme, H., Cloutier, P. A., Connerney, J. E. P., et al. (2001). Probing Mars' crustal. *Journal of Geophysical Research*, *106*, 23,419–23,428. https://doi.org/10.1029/2000JE001435

Němec, F., Morgan, D. D., Gurnett, D. A., & Duru, F. (2010). Nightside ionosphere of Mars: Radar soundings by the Mars Express spacecraft. *Journal of Geophysical Research*, *115*, E12009. https://doi.org/10.1029/2010JE003663

Němec, F., Morgan, D. D., Gurnett, D. A., Duru, F., & Truhlík, V. (2011). Dayside ionosphere of Mars: Empirical model based on data from the MARSIS instrument. *Journal of Geophysical Research*, *116*, E07003. https://doi.org/10.1029/2010JE003789

Ness, N. F., Acuña, M. H., Connerney, J. E. P., Kliore, A. J., Breus, T. K., Krymskii, A. M., et al. (2000). Effects of magnetic anomalies discovered at Mars on the structure of the Martian ionosphere and solar wind interaction as follows from radio occultation experiments. *Journal of Geophysical Research*, *105*, 15,991–16,004. https://doi.org/10.1029/1999JA000212

Nielsen, E., Fraenz, M., Zou, H., Wang, J.-S., Gurnett, D. A., Kirchner, D. L., et al. (2007). Local plasma processes and enhanced electron densities in the lower ionosphere in magnetic cusp regions on Mars. *Planetary and Space Science*, *55*, 2164–2172. https://doi.org/10.1016/j.pss.2007.07.003

Pätzold, M., Häusler, B., Tyler, G. L., Andert, T., Asmar, S. W., Bird, M. K., et al. (2016). Mars Express 10 years at Mars: Observations by the Mars Express Radio Science Experiment (MaRS). *Planetary and Space Science*, *127*, 44–90.

Phillips, J. L., Luhmann, J. G., & Russell, C. T. (1984). Growth and maintenance of large-scale magnetic fields in the dayside Venus ionosphere. *Journal of Geophysical Research*, *89*, 10,676–10,684.

Ramírez-Nicolás, M., Sánchez-Cano, B., Witasse, O., Blelly, P.-L., Vázquez, L., & Lester, M (2016). The effect of the induced magnetic field on the electron density vertical profile of the Mars' ionosphere: A Mars Express MARSIS radar data analysis and interpretation, a case study. *Planetary and Space Science*, *126*, 49–62.

Ramstad, R., Barabash, S., Futaana, Y., Nilsson, H., Wang, X.-D., & Holmström, M. (2015). The Martian atmospheric ion escape rate dependence on solar wind and solar EUV conditions: 1. Seven years of Mars Express observations. *Journal of Geophysical Research: Planets*, *120*, 1298–1309. https://doi.org/10.1002/2015JE004816

Safaeinili, A., Kofman, W., Mouginot, J., Gim, Y., Herique, A., Ivanov, A. B., et al. (2007). Estimation of the total electron content of the Martian ionosphere using radar sounder surface echoes. *Geophysical Research Letters*, *34*, L23204. https://doi.org/10.1029/2007GL032154

Sakai, S., Andersson, L., Cravens, T. E., Mitchell, D. L., Mazelle, C., Rahmati, A., et al. (2016). *Journal of Geophysical Research: Space Physics*, *121*, 7049–7066. https://doi.org/10.1002/2016JA022782

Schunk, R. W. (1977). Mathematical structure of transport equations for multispecies flows. *Reviews of Geophysics and Space Physics*, *15*, 429–445.

Shinagawa, H., & Cravens, T. E. (1988). A one-dimensional multispecies magnetohydrodynamic model of the dayside ionosphere of Venus. *Journal of Geophysical Research*, *93*, 11,263–11,277.

Shinagawa, H., & Cravens, T. E. (1989). A one-dimensional multispecies magnetohydrodynamic model of the dayside ionosphere of Mars. *Journal of Geophysical Research*, *94*, 6506–6516.

Shinagawa, H., Cravens, T. E., & Nagy, A. F. (1987). A one-dimensional time-dependent model of the magnetized ionosphere of Venus. *Journal of Geophysical Research*, *92*, 7317–7330.

Steckiewicz, M., Garnier, P., André, N., Mitchell, D. L., Andersson, L., Penou, E., et al. (2017). Comparative study of the Martian suprathermal electron depletions based on Mars Global Surveyor, Mars Express, and Mars Atmosphere and Volatile EvolutioN mission observations. *Journal of Geophysical Research: Space Physics*, *122*, 857–873. https://doi.org/10.1002/2016JA023205

Steckiewicz, M., Mazelle, C., Garnier, P., André, N., Penou, E., Beth, A., et al. (2015). Altitude dependence of nightside Martian suprathermal electron depletions as revealed by MAVEN observations. *Geophysical Research Letters*, *42*, 8877–8884. https://doi.org/10.1002/2015GL065257

Tyler, G. L., Balmino, G., Hinson, D. P., Sjogren, W. L., Smith, D. E., Simpson, R. A., et al. (2001). Radio science observations with Mars Global Surveyor: Orbit insertion through one Mars year in mapping orbit. *Journal of Geophysical Research*, *106*, 23,327–23,348. https://doi.org/10.1029/2000JE001348

Vogt, M. F., Withers, P., Mahaffy, P. R., Benna, M., Elrod, M. K., Halekas, J. S., et al. (2015). Ionopause-like density gradients in the Martian ionosphere: A first look with MAVEN. *Geophysical Research Letters*, *42*, 8885–8893. https://doi.org/10.1002/2015GL065269

Weber, T., Brain, D., Mitchell, D., Xu, S., Connerney, J., & Halekas, J. (2017). Characterization of low-altitude nightside Martian magnetic topology using electron pitch angle distributions. *Journal of Geophysical Research: Space Physics*, *122*, 9777–9789. https://doi.org/10.1002/2017JA024491

Withers, P., Fillingim, M. O., Lillis, R. J., HäUsler, B., Hinson, D. P., Tyler, G. L., et al. (2012). Observations of the nightside ionosphere of Mars by the Mars Express Radio Science Experiment (MaRS). *Journal of Geophysical Research*, *117*, A12307. https://doi.org/10.1029/2012JA018185

Withers, P., Vogt, M., Mahaffy, P., Benna, M., Elrod, M., & Jakosky, B. (2015). Changes in the thermosphere and ionosphere of Mars from Viking to MAVEN. *Geophysical Research Letters*, *42*, 9071–9079. https://doi.org/10.1002/2015GL065985

Withers, P., Vogt, M., Mayyasi, M., Mahaffy, P., Benna, M., Elrod, M., et al. (2015). Comparison of model predictions for the composition of the ionosphere of Mars to MAVEN NGIMS data. *Geophysical Research Letters*, *42*, 8966–8976. https://doi.org/10.1002/2015GL065205

Xu, S., Mitchell, D., Liemohn, M., Fang, X., Ma, Y., Luhmann, J., et al. (2017). Martian low-altitude magnetic topology deduced from MAVEN/SWEA observations. *Journal of Geophysical Research: Space Physics*, *122*, 1831–1852. https://doi.org/10.1002/2016JA023467

Xu, S., Mitchell, D., Luhmann, J., Ma, Y., Fang, X., Harada, Y., et al. (2017). High-altitude closed magnetic loops at Mars observed by MAVEN. *Geophysical Research Letters*, *44*, 11,229–11,238. https://doi.org/10.1002/2017GL075831

Xu, S., Thiemann, E., Mitchell, D., Eparvier, F., Pawlowski, D., Benna, M., et al. (2018). Observations and modeling of the Mars low-altitude ionospheric response to the 10 September 2017 X-Class solar flare. *Geophysical Research Letters*, *45*, 7382–7390. https://doi.org/10.1029/2018GL078524